 Hot Paper

Engineering Phi29-DNAP Variants for Customized DNA Hydrogel Materials

Philipp Gaspers,^[a] Phillip Lemke,^[a] André Delavault,^[a] Carmen M. Domínguez,^[a]
 Kersten S. Rabe,^[a] and Christof M. Niemeyer^{*[a]}

DNA hydrogels, which hold potential for use in medicine, biosensors, and tissue engineering, can be produced through enzymatic rolling circle amplification (RCA) using phi29 DNA polymerase (DNAP). This paper introduces new DNAP variants designed for RCA-based DNA hydrogel production, featuring enzymes with modified DNA binding, enhanced thermostability, reduced exonuclease activity, and protein tags for fluorescence detection or specific immobilization. We evaluated these enzymes by quantifying DNA output via quantitative PCR

(qPCR) and assessing hydrogel mechanical properties through micromechanical indentation. The results showed that most variants generated similar DNA amounts and hydrogels with comparable mechanical properties. Additionally, all variants successfully incorporated non-natural nucleotides, such as base-modified dGTP derivatives and 2'fluoro-dGTP, during RCA. This study's robust analytical approach offers a strong foundation for selecting new enzymes and producing DNA hydrogels with tailored material properties.

Introduction

Since the early conceptual work of Nadrian Seeman in the 1980s,^[1] the concept of DNA-based materials has developed into a highly innovative and dynamic field of research at the interface of chemistry, materials science, biotechnology and nanotechnology.^[2] From today's perspective, the broad international research and development of DNA materials can be divided into various sub-disciplines, ranging from pure "structural DNA nanotechnology" to DNA-based hydrogel materials and composites with proteins and nanoparticles.^[2c] The development of DNA-based polymeric materials^[3] was initiated by Dan Luo's group with the demonstration that synthetic branched DNA oligonucleotide building blocks can be assembled into macroscopic hydrogel materials by hybridization/ligation.^[4] Since then, a variety of methods have been developed for the production of DNA hydrogels, which, for example, include the enzymatic linking of linear oligonucleotides, the use of cytosine-rich DNA sequences to form tetrameric structures called i-motifs, which are induced to self-assemble by pH changes, or the use of a clamped hybridization chain reaction of individual DNA units, in which initially blocked self-complementary sequences are opened by a catalytically

active initiator strand and triggered into a polymerization reaction.^[2c,3a] A more economically favorable approach is to produce DNA polymers by enzymatic extension of primer oligonucleotides, which is efficiently possible in particular by the so-called 'rolling circle amplification' (RCA). This leads to entangled networks of DNA strands that have a very soft consistency and often reveal shape memory persistence.^[5] Importantly, the RCA method can be directly transferred to other scaffolds and hydrogels. Since the generated DNA backbone consists of concatemeric repeats of the template sequence, the specific design of the template allows for easy customization of the resulting materials properties.^[6] Furthermore, the RCA process can be combined with artificial materials such as nanoparticles to create complex DNA composite materials.^[7] RCA can even be used to produce mesoscopic structures with distinct morphologies, often referred to as "DNA nanoflowers," making this method highly versatile.^[8] These structures are about 1–2 μm in size and are readily taken up by mammalian cells, opening up applications for drug delivery^[8b] and protein encapsulation^[9] during the polymerization process. In general, DNA hydrogels have recently attracted increasing interest because these biopolymers can be programmed very efficiently via their nucleic acid sequence to install, in addition to shape memory persistence, molecular recognition capabilities and stimulus sensitivity, for example to facilitate their biodegradation by enzymes. These unique material properties are of great importance for a variety of life science applications, especially in biomedical fields like drug delivery, tissue engineering and biosensing.^[2c,3a,b,10]

The RCA underlying these materials produces long concatemeric single-stranded DNA (ssDNA) chains (>20000 nt) starting from a primer hybridized with a short circular ssDNA template using the enzyme phi29 DNA polymerase (DNAP, Figure 1A), which, due to its extremely high processivity, enables the cost-effective production of large amounts of DNA under isothermal conditions.^[5,11] Considering the multiple possibilities for *in vivo*

[a] P. Gaspers, P. Lemke, A. Delavault, C. M. Domínguez, K. S. Rabe, C. M. Niemeyer
 Institute for Biological Interfaces 1 (IBG 1), Karlsruhe Institute of Technology (KIT), Hermann-von-Helmholtz-Platz 1, 76344 Eggenstein-Leopoldshafen, Germany
 E-mail: niemeyer@kit.edu

Supporting information for this article is available on the WWW under <https://doi.org/10.1002/chem.202403047>

© 2024 The Author(s). Chemistry - A European Journal published by Wiley-VCH GmbH. This is an open access article under the terms of the Creative Commons Attribution Non-Commercial NoDerivs License, which permits use and distribution in any medium, provided the original work is properly cited, the use is non-commercial and no modifications or adaptations are made.

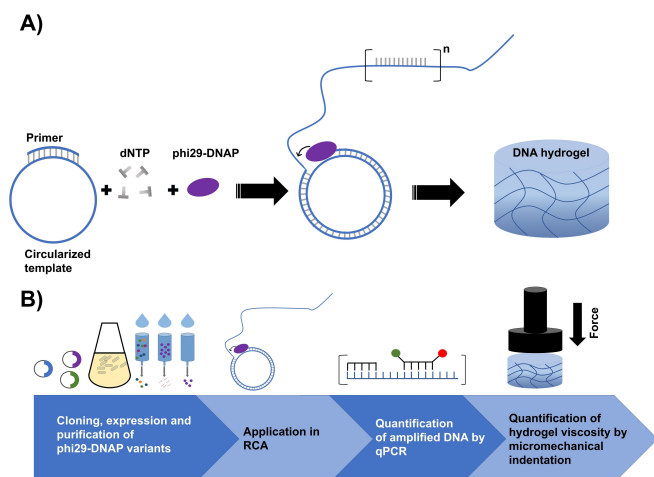


Figure 1. Conceptual basis of this work: A) Schematic representation of rolling circle amplification (RCA). Starting from an oligonucleotide primer that is hybridized to a circular template, phi29-DNAP performs DNA amplification. Once the polymerase reaches the primer terminus again, the enzyme displaces the previously synthesized DNA which results in the generation of long concatemers of ssDNA of up to 20000 nt in length that can form DNA hydrogels due to physical entanglement. B) Workflow of the production and investigation of DNAP variants for the production of RCA-based DNA hydrogel materials.

applications of DNA hydrogels, the biochemical modification of the polymers with non-natural nucleotides such as base-modified 2'-deoxyribonucleoside triphosphates,^[12] could be an interesting perspective, e.g. to improve the nuclease resistance of the materials and thus their residence time in living systems.

Indeed, due to the tremendous advances in organic synthesis and polymerase engineering, co-polymerization of modified deoxy-nucleoside triphosphates (dN*TPs) has emerged as a versatile and practical method to expand the chemical repertoire of intrinsically low-functionality nucleic acids.^[13] However, their use for *in situ* functionalization of DNA materials is not well investigated.^[14]

The enzyme phi29-DNAP is very well studied. It exhibits a robust exonuclease and proofreading activity that reduces the probability of erroneous nucleotide insertion during polymerization by a factor of 10^4 to 10^6 .^[15] While this capability is advantageous for applications requiring reliable amplification, it reduces the insertion efficiency and choice of nucleotide analogues that might be incorporated and can lead to complete suppression of RCA.^[16] In recent years, several new phi29-DNAP variants have been developed to generally increase the DNA yield of RCA or the synthesis efficiency of 'xenonucleic acids' (XNA, that contain non-natural nucleotide analogues). For example, de Vega *et al.* fused phi29-DNAP with a DNA-binding domain from *Methanopyrus kandleri* (*M. kandleri*), which increased the yield of multiply primed RCA and multiple displacement amplification (MDA) by fourfold.^[17] A different approach was taken by Povilaitis *et al.* who used the complementary self-replication (CSR) technique to produce a more thermostable variant, which also showed greatly improved amplification performance in MDA.^[18] An exonuclease-deficient variant of phi29-DNAP (D12A) was used to catalyze the

synthesis of short XNA fragments containing 2'-fluoro DNA or 1,5-anhydrohexitic nucleic acid,^[19] which show great promise as nuclease-resistant oligonucleotides for clinical therapies.^[20] However, since the previously used mutant D12A had lost the ability for strand displacement, it cannot perform RCA. Some other mutants, such as phi29-T15I, show significantly reduced exonuclease activity, but can still be used for RCA.^[21]




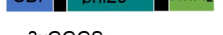


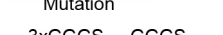
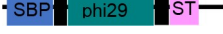
To build on these studies and contribute to new innovations for the research field of functional DNA materials, we report here on the evaluation of phi29-DNAP variants for the production of functional DNA hydrogels (Figure 1B). These include variants with reduced exonuclease activity as well as new fusion enzymes with affinity- or fluorescent markers. Specifically, we describe a variant that is labelled with the red fluorescent protein (RFP) and could be used for localization experiments on hydrogel formation in microscopic cavities. Furthermore, as DNA hydrogels are increasingly being considered for microfluidic applications,^[22] we describe a variant functionalized with domains of the SpyTag/SpyCatcher coupling system^[23] to realize quick and efficient immobilization of the polymerase on surfaces. To characterize the new phi29-DNAP variants, we investigated their ability to generate DNA hydrogels by acquiring quantitative data on the processivity of the variants using a recently developed quantitative polymerase chain reaction (qPCR)-based method.^[24] Furthermore, we utilized a newly developed micromechanical indentation platform^[25] for the quantitative evaluation of the mechanical properties of the formed DNA hydrogels.

Discussion

Production of Enzymes

To investigate new phi29-DNAP variants for the production of DNA hydrogels, we selected several enzymes from the literature and genetically tagged them with the above-mentioned markers (Table 1, see also Table S1, in the Supporting Information). To produce selected phi29-DNAP variants, we first fused the wild-type phi29-DNAP gene (phi29-WT) to a streptavidin-binding peptide tag (SBP-tag) for easier purification and inserted it into a pET 22b+ vector. This construct then served as the backbone for generating several phi29-DNAP variants: phi29-H, containing a C-terminal DNA binding motif,^[17] phi29-M5, containing eight point mutations for improved thermostability,^[18] phi29-ΔE which displays a strongly reduced exonuclease activity due to the point mutation T15I,^[21] the two variants phi29-ST and phi29-SC, which contain a C-terminal SpyTag or SpyCatcher, respectively, for immobilization purposes, and phi29-RFP containing a red fluorescent protein (RFP) fused to the N-terminus of the enzyme. The variants were heterologously expressed in *E. coli* BL21 and purified to near homogeneity using SBP affinity chromatography. A representative sodium dodecyl sulphate polyacrylamide gel electrophoresis (SDS-PAGE) analysis of the purified proteins is shown in Figure S1, Supporting Information. Since phi29-H, phi29-SC and phi29-RFP showed slight impurities, we used calibration curves

Table 1. Overview of the phi29-DNAP variants used in this study. All variants except phi29-NEB were cloned into a pET-22b+ containing a pBR322 ori, an isopropyl- β -D-thiogalactopyranoside (IPTG) inducible T7 promoter and an ampicillin resistance gene. All phi29-DNAP variants produced in this study contain a streptavidin-binding peptide (SBP) tag connected via a 3x GGGS linker to the polymerase for chromatographic purification. MW: Molecular weight.

phi29 DNAP Variant	Schematic illustration of protein sequence	Modification/Feature	MW (kDa)	Yield (mg/L)	Source
phi29-NEB		Wild-type produced by NEB	67	-	NEB
phi29-WT		Wild-type	71.8	23	This study
phi29-H		C-terminal HhH ₂ domain from <i>M. kandleri</i> for enhanced DNA binding	78.5	6.5	This study following reference ^[17]
phi29-M5		Mutations: M8R, V51 A, M97T, G197D, E221 K, Q497P, K512E and F526 L for higher thermostability	71.8	65	This study following reference ^[18]
phi29- Δ E		Mutation: T15I for impaired exonuclease activity	71.8	16.3	This study following reference ^[21]
phi29-ST		C-terminal ST-tag that binds to SC-tagged proteins	73.6	14.6	This study
phi29-SC		C-terminal SC-tag that binds to ST-tagged proteins	84.3	13.5	This study
phi29-RFP		N-terminal RFP-tag, λ_{exc} 590, λ_{em} 610	97.1	18.5	This study

with known concentrations of bovine serum albumin (BSA) to obtain the exact concentration of DNAP for the upcoming RCA investigations (Figure S2). Of note, the observed expression yields (Table 1) varied widely between the variants, ranging from 6.5 mg/L for phi29-H to a maximum of 70 mg/L of expression culture for phi29-M5. Overall, all yields were sufficiently high to provide enough material for further characterization of the enzymes in the RCA process.

Functional Characterization of the Various Phi29-DNAP Variants

To investigate the processivity of the different phi29-DNAP variants in RCA-based hydrogel synthesis, we first aimed to develop a real-time fluorescent RCA assay (Figure S3) using SYBR Green I (SG) to stain the amplified DNA, as this would have the advantage of rapidly assessing enzyme activity in real-time and at high throughput. SG intercalates into newly synthesized double-stranded DNA (dsDNA) formed either by secondary structures or by inter- and intramolecular hybridization as ssDNA concentrates, resulting in a 1000-fold increase in SG fluorescence that can be measured with a fluorescence plate reader. Specifically, a circular template was used (hereafter referred to as template A, for details on secondary structure prediction and characterization of the cyclized template A, see Figures S4 and S5). To establish the SG assay (Figure S3), screenings were first performed with herring sperm DNA, which

showed that a linear increase of the fluorescence signal with DNA concentration could only be achieved for very high SG concentrations and for a relatively low DNA concentration range of 0–50 ng/ μ L. The use of these experimental conditions proved to be unsuitable for real-time measurement of product DNA formed during RCA, as high SG levels inhibited the RCA process. We therefore analyzed the activity and processivity of phi29-DNAP using a recently developed qPCR protocol (Figures 2A, 2B), which allows the accurate quantification of DNA.^[24]

To assess the dynamic range of the RCA assay, four different dilutions (0.05, 0.1, 0.2 and 0.4 U/ μ L) of commercial phi29-DNAP from New England Biolabs (phi29-NEB), which according to the manufacturer has an activity of 10 U/ μ L in the stock solution were used in 72 hour reactions in which the other reagent concentrations were kept constant (adjusted dNTP mix to match the composition of the amplicon sequence G:C:T:A (1.8, 1.25, 1.11 and 0.88 mM), primers (100 nM) and cyclized template (50 nM)). As expected, DNA production strongly depended on the concentration of phi29-NEB used, in particular, during the initial phase of RCA (Figure 2C). The data also showed that amplification slowed down considerably after approximately 24 hours of incubation, regardless of the amount of enzyme used, resulting in only a slight increase in final concentration by the end of the experiment. Importantly, samples with higher phi29-NEB concentrations (0.2 and 0.4 U/ μ L) showed significantly higher RCA final product concentrations than those with lower concentrations (0.05 and 0.1 U/ μ L) (Figure 2D, see also Figure S7). This suggested that the decrease

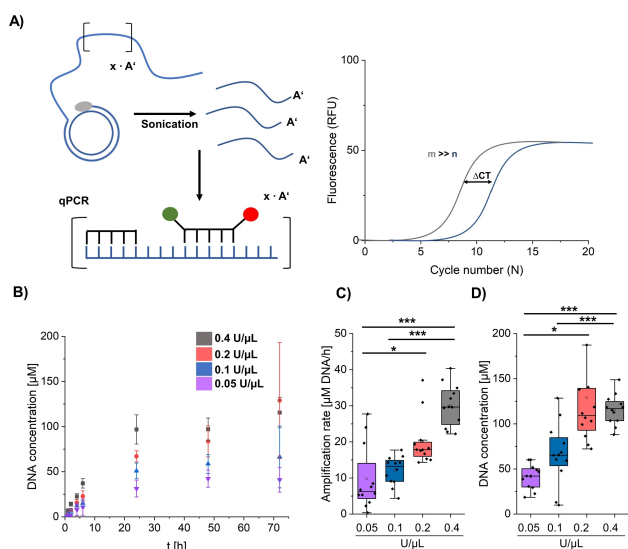


Figure 2. Evaluation of the dynamic range of RCA using phi29-NEB. A) Principle of the qPCR analysis for quantification of the RCA product.^[24] Long RCA amplicons are cleaved into smaller fragments by sonication and subsequently quantified using a TaqMan probe containing a fluorescent reporter and a quencher dye, which are separated during amplification by the Taq-DNAP. The fluorescence signal is correlated with background fluorescence and plotted as a ΔCt value that indicates at which PCR cycle the measurement signal appears compared to the background. Absolute quantification was achieved by external calibration curves (Figure S6). B) Quantification of the produced DNA during RCA over a time period of 72 h using variable amounts of commercial phi29-NEB under RCA standard conditions C) Box plot representation of the initial amplification rate observed for variable amounts of phi29-NEB during the first six hours of RCA and (D) final RCA product concentration obtained after 72 h of RCA. For corresponding data of 24 h and 48 h, see Figure S7. Error bars were obtained from at least two independent experiments. Data were analysed using a Kruskal-Wallis test followed by a Dunn-Bonferroni test for pairwise comparisons. * $P < 0.05$, ** $P < 0.01$ and *** $P < 0.001$.

in amplification is not due to depletion of reagents, such as dNTPs, but rather due to the loss of enzyme activity in the developing DNA hydrogel matrix. Overall, the results clearly demonstrated that the polymerization assay can effectively distinguish between different activities, making it suitable for comparing new phi29-DNAP variants based on their capacity to produce DNA hydrogels.

In order to use the dynamic range of the RCA assay determined with phi29-NEB for the activity determinations of our self-produced phi29-DNAP variants, we evaluated the molar concentration of phi29-NEB by SDS-PAGE, which resulted in a value of about 40 nM for a concentration of 0.4 U/ μL in the reaction mixture (for details, see RCA standard conditions specified in the SI). Subsequent RCA experiments with the novel phi29-DNAP variants were then performed with an enzyme concentration of 20 nM to detect differences in processivity. The results for the amplification rate and final RCA product concentrations after 72 h for each variant are shown in Figures 3A–3I. Corresponding data obtained after 24 h and 48 h are shown in Figure S8. We observed that phi29-WT (Figure 3A) had a similar amplification rate and final RCA product concentration after 72 hours as the above studied phi29-NEB (Figures 2B–D). This demonstrated not only that no loss of

activity results from the SBP tag at the enzyme's N-terminus, but also that the protocols applied here for recombinant expression and purification were suitable for effective production of active polymerase variants.

In contrast to the literature,^[17,18] variants phi29-H (Figure 3B) and -M5 (Figure 3C) showed neither an increased DNA amplification rate nor a significant increase in the final RCA product concentration after 72 hours. For the phi29-H variant, this could be due to its increased DNA binding capacity, which might favor entrapment of the enzyme within the developing DNA hydrogel matrix, thereby impairing its ability to bind and amplify free RCA templates. This hypothesis is consistent with results reported in the literature^[17] concerning the study of a variant that had two DNA binding domains at the C-terminus (phi29-HI). This variant showed a lower DNA yield in the amplification of genomic DNA towards the end of the experiment, although amplification was better in the early phases. The authors assumed that the presence of two DNA-binding domains leads to immobilization of the enzyme, as binding is enhanced once a certain amount of DNA is present.^[17] Although this effect did not occur in the previous study with the phi29-H variant, it may be more pronounced in our work, as the very long DNA segments form an interwoven 3D network, in which the local concentration of DNA and also the constraints for diffusion are likely to be higher than in the amplification of genomic DNA. No comparable literature data are known for phi29-M5, as it was only examined in the MDA assay, where it showed a 5-fold increase in DNA yield compared to the wild type.^[18] There, the strongest increase in amplification efficiency was observed at elevated temperatures of 40 °C, which should promote amplification of templates with high GC content. The decrease in processivity observed here could therefore be due to the lower reaction temperature in our assay (30 °C).

The phi29- ΔE variant (Figure 3D) showed significantly lower RCA product formation throughout the time period studied, mirroring the slight decrease (by 10%) in RCA performance reported in the literature when using primed M13 phage DNA.^[21] Another reason that might explain the low DNA yield is the fourfold lower fidelity of phi29- ΔE compared to the wild-type enzyme. The introduction of mismatched nucleotides during amplification could interfere with primer and TaqMan probe binding during qPCR, which could affect the correctness of qPCR quantification.

For the SpyTag-modified phi29-ST variant (Figure 3E), no significant difference in the initial amplification rate and final RCA product concentration was observed compared to phi29-WT. This indicates that a fusion of short peptide domains (ST contains 13 amino acids) at the C-terminus of the enzyme is possible without significantly affecting the activity. In contrast, phi29-SC (Figure 3F), which was fused at the C-terminus with the relatively large SpyCatcher domain (12.3 kDa), showed a significantly reduced polymerization efficiency. In comparison to phi29-WT, only 50% of the amplification rate and the final RCA product concentration could be achieved. This observation could be related to the fact that the fusion of the bulky SC domain could interfere with the proper folding of the enzyme and/or disrupt the DNA-binding ability of the enzyme, since the

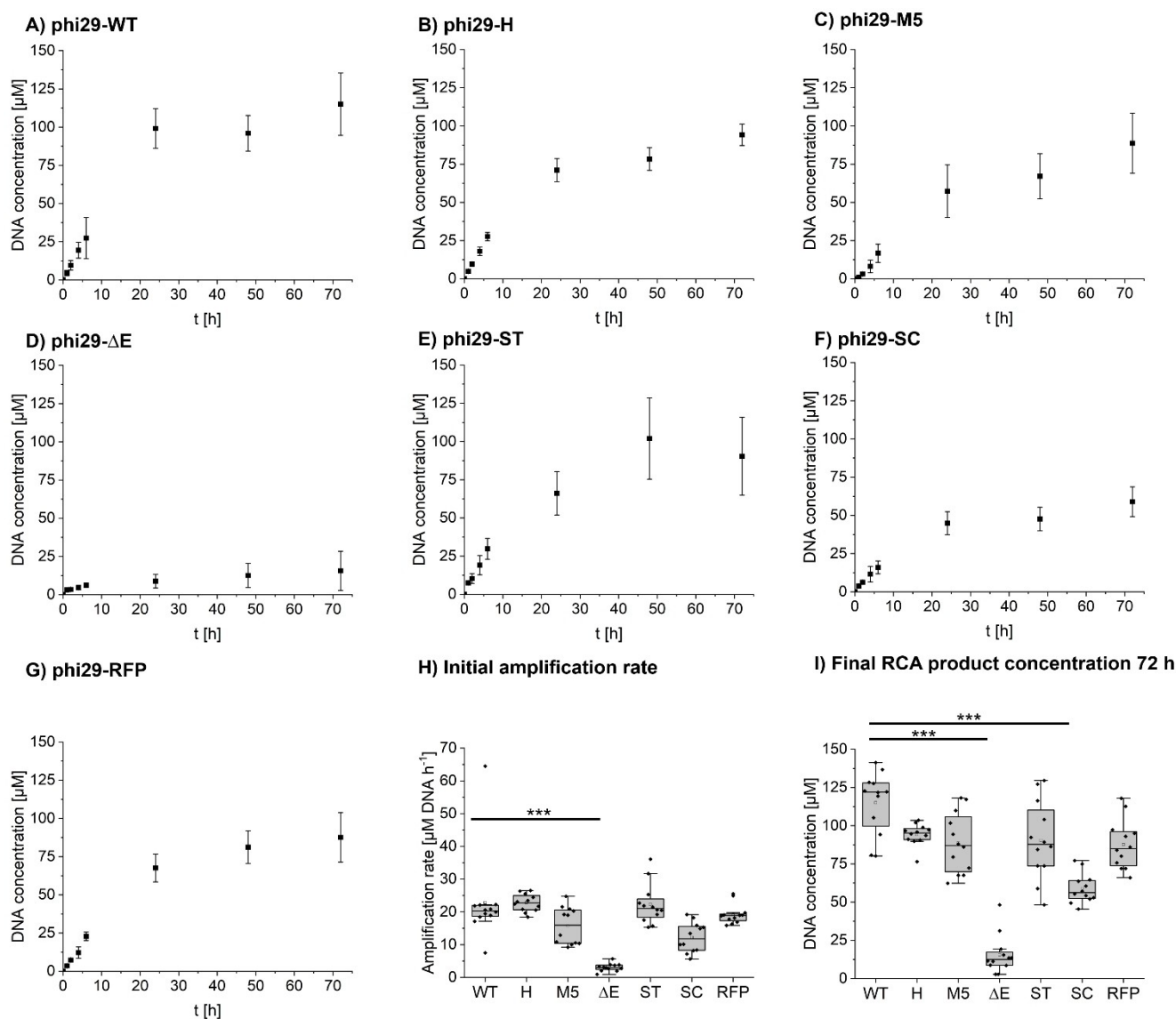


Figure 3. Comparison of DNA yields produced by different phi29-DNAP variants in RCA as determined by qPCR. A–G) 20 nM of each phi29-DNAP variant was used to perform RCA under standard reaction conditions as described in the Materials and Methods section. Samples were taken at different time points, the reaction was stopped by heat denaturation and the amount of DNA product formed was quantified by qPCR. H) Boxplot representation of the amplification rate within the first 6 hours of the reaction, and I) boxplot representation of the final product concentration after 72 hours of RCA for all phi29-DNAP variants. For corresponding data showing DNA concentration after 24 and 48 hours, see Figure S8. The error bars were obtained from at least two independent experiments. Data were analysed using a Kruskal-Wallis test followed by a Dunn-Bonferroni test for pairwise comparisons. * $P < 0.05$, ** $P < 0.01$ and *** $P < 0.001$.

thumb subdomain of phi29-DNAP is located at the C-terminus.^[26]

In contrast to the SC/ST-labelled variants, phi29-RFP (Figure 3G) contains a voluminous red fluorescent protein (MW RFP = 27 kDa) at the N-terminus. In this case, qPCR results showed no reduction in amplification rate and only a slight but not significant reduction in final RCA product concentration, suggesting that the N-terminus may be more suitable for fusion of additional protein domains. To evaluate if phi29-RFP shows fluorescent properties we recorded the excitation and emission spectra. Peak fluorescence values of 590 nm for excitation and 610 nm for emission clearly indicated, that the RFP-tag is functional (Figure S9).

We also investigated the binding tag functionality of the phi29-ST and phi29-SC variants. Here, electrophoretic binding studies with a complementary labelled protein showed that both phi29-ST and phi29-SC exhibited unrestricted binding functionality, leading to an almost complete coupling with the binding partner after only 10 minutes (Figure S10). We also investigated whether the polymerase activity of these variants is affected when the enzymes are immobilized on a surface. To this end, phi29-ST and, as a control, phi29-WT were immobilized onto epoxy-polystyrene beads that had previously been coated with SC proteins.^[27] Quantification of the coupling process by supernatant depletion indicated a substantial binding efficiency for phi29-ST (about $9.1 \pm 0.05 \mu\text{g enzyme/mg beads}$), whereas

lower amounts (about $6.0 \pm 0.1 \mu\text{g}$) of enzyme were bound per mg beads in the case of phi29-WT (Figure S11). Functional testing the enzyme-coated beads in RCA revealed that the beads containing phi29-ST led to an about 10-fold higher amount of product than the beads containing non-specifically adsorbed phi29-WT. Given that the surface loading of the phi29-ST-beads was only about 1.5-fold as high as of the phi29-WT-beads, this result suggested that directional coupling via the SC/ST system led to a more active enzyme on the bead surface. However, comparison with non-immobilized phi29-ST (Figure 3) showed that the enzyme activity decreases more than fivefold due to surface immobilization. Based on the considerations described above, it can be speculated that the enormous steric bulk of the SpyCatcher-containing surface in close proximity to the C-terminus of the enzyme is responsible for this negative effect, so that the use of N-terminally positioned ST could lead to improvements.

To complete the characterization of the RCA materials, we also investigated the viscoelastic properties of DNA hydrogels produced by the various phi29-DNAP. To this end, a novel micromechanical indentation platform developed recently in our lab was used (Figure S12).^[25] In brief, 75 μL of DNA hydrogels generated in typical 72 h reactions were transferred into a sample holder (4.5 mm diameter, 4 mm depth) and apparent viscosity of the samples were measured by slowly inserting a plunger into the gel with a speed of 1 mm/s. The resulting force-displacement curves allowed the apparent viscosity of the samples to be calculated using a calibration function. The resulting data showed that most of the DNA hydrogels produced by the different phi29-DNAP variants had quite similar apparent viscosities (Figure S12C).

Incorporation of Non-Natural Nucleotides

It has recently been shown on a qualitative level that the wild-type phi29-DNAP is capable to incorporate artificial dUTP and dCTP nucleotide analogues during DNA amplification to synthesize DNA nanoflowers containing chemical handles for subsequent functionalization using bioorthogonal reactions.^[14b] However, data regarding the efficiency and impact on the amplification performance in the context of DNA hydrogels is currently lacking. To evaluate the potential of our newly engineered phi29-DNAP variants for the incorporation of artificial nucleotides, the enzymes were subjected to testing with various types of nucleotides (Figure 4).

In comparison to standard dNTPs, such as dGTP (1), modified nucleotides were used that contain an alkyne or ethynyl group at the 5-position of the pyrimidine base of dUTP (2,3) and enable the coupling of molecules with an azide group via a copper(I)-catalyzed alkyne-azide cycloaddition (CuAAC). These nucleotides had previously been used in the synthesis of chemically modifiable DNA nanoflowers.^[14b] Biotin-16-dUTP (4) harbours a biotin group which is connected by a linker to the 5-position of the pyrimidine base of dUTP. This nucleotide would allow the modification of the DNA hydrogel via streptavidin conjugates. 2'fluoro-dGTP (5) and 2'OMe-dGTP (6) contain a

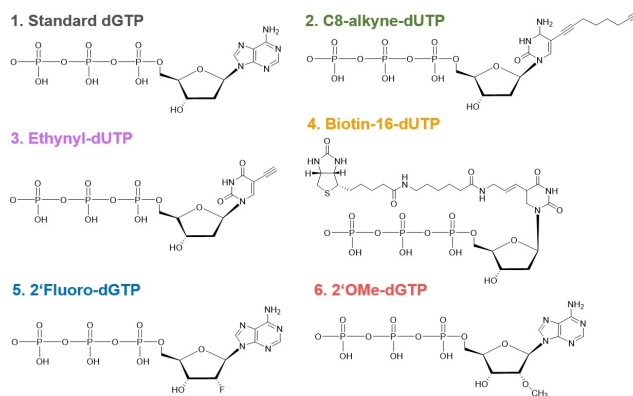


Figure 4. Chemical structures of the nucleotides selected for this study for incorporation by phi29-DNAP variants in the RCA 1: Deoxyguanosine triphosphate (dGTP), as an example of natural nucleotides used for the RCA. 2,3: Deoxyuridine triphosphate with an alkyne modification at the 5-position of the pyrimidine base. 4: Deoxyuridine triphosphate with a linker-connected biotin group at the 5-position of the pyrimidine base. 5,6: Fluoro- or methoxy group at the 2'-position of the GTP-ribose.

fluorine or methoxy group, respectively, at the 2' position of the ribose. These nucleotides can confer increased resistance to nucleases and are therefore promising for the production of DNA nanomaterials for cell culture applications or oligonucleotides for therapeutic use. However, the modifications often pose a challenge as they lead to steric conflicts with the active site of most polymerases.^[20,28]

To determine whether the new phi29-DNAP variants developed here are capable of incorporating the nucleotides shown in Figure 4, we investigated the influence of these nucleotides on RCA in typical 72 h reactions and characterized the generated DNA hydrogels by qPCR (Figure 5). It should be noted in this approach that some non-natural nucleotides, such as 2'fluoro- and 2'OMe-dNTP, can influence Watson-Crick hydrogen bonding and base-stacking interactions in such a way that the enzymatic reading by polymerases, and thus the quantification of DNA concentration using qPCR (Figure 5), could be affected. Therefore, in the course of the investigations described below, additional electrophoretic analyses of the RCA samples were consistently performed to verify the formation of the typical high-molecular-weight products. First, we looked at dUTP (2,3,4 in Figure 4), which allow post-synthetic modification of the introduced group after RCA. For this purpose, 1 % of the natural dTTP in the reaction mixture was replaced by the dUTP derivative. The qPCR analysis showed that the RCA performed with C8-alkyne- or ethynyl-dUTP produced similar amounts of DNA for all tested phi29-DNAP variants as with the standard dNTP mix. However, some variants showed reduced processivity (phi29-WT, phi29-H, phi29-SC), but with no statistical significance. For the RCA performed with biotin-16-dUTP, qPCR analysis revealed that this nucleotide was not incorporated by phi29- ΔE . A slight but not significant (approximately 1.5-fold) decreased RCA product yield was observed for the phi29-WT, phi29-H and phi29-SC variants, as compared to the RCA products generated under standard conditions (Figure 5A-5F, column 1 vs 4). This reduction could possibly be due to steric

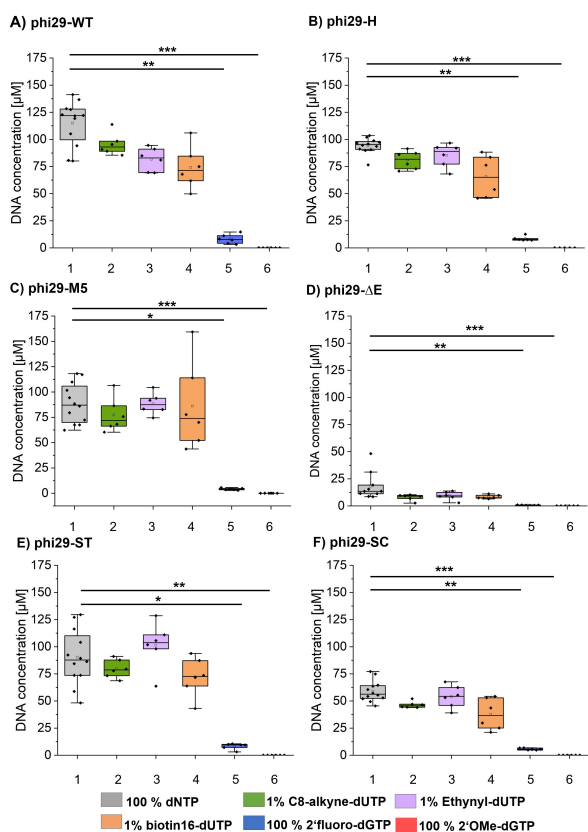


Figure 5. qPCR-based quantification of RCA product obtained after 72 hours with different phi29-DNAP variants using artificial nucleotides. A–F) The effects of artificial nucleotides on RCA productivity were investigated with 20 nM of phi29-DNAP using different nucleotide reaction mixtures: 1, gray: 100% standard nucleotides; 2, green: C8-alkyne-dUTP; 3, purple: ethynyl-dUTP; 4, orange: biotin-16-dUTP; 5, blue: 2'fluoro-dGTP or 6, red: 2'OMe-dGTP. The error bars were obtained from at least two independent experiments. Data was analysed using a Kruskal-Wallis test followed by a Dunn-Bonferroni test for pairwise comparisons. * $P < 0.05$, ** $P < 0.01$ and *** $P < 0.001$.

hindrance caused by the size of the biotin group, although it is connected to the nucleobase via a long linker.

Electrophoretic analyses of the RCA samples showed the typical high molecular weight products formed when using the natural nucleotides for both the alkyne-modified dUTP (Figure S13) and the biotin-modified dUTP (Figure S14). To verify that artificial nucleotides were incorporated during DNA amplification, in the case of the alkynyl derivatives, we used the RCA product to perform a CuAAC click reaction with an azide-modified Cy3 (Az^{Cy3}) dye (Figure S13). In the case of the biotin derivative, the RCA product was incubated post-synthetically with a Cy3-labelled streptavidin (STV^{Cy3} , Figure S14). Indeed, fluorescence analysis of the gel bands clearly revealed the expected Cy3 fluorescence in the respective RCA samples. To obtain a rough estimate of the labelling efficiency, we calculated the ratio of fluorescence intensities obtained by image analysis of electrophoretic examination from the lanes with the DNA dye SYBR™ safe and the Cy3 dye, respectively (Figure S15). The ratios obtained showed that for all enzymes tested, the DNA hydrogels with C8-alkyne-dUTP showed a

slightly stronger phi modification than the hydrogels modified with ethynyl-dUTP (Figure 6). This could be due to the longer linker of the C8-alkyne-dUTP, which allows better accessibility for the post-synthetic modification with Az^{Cy3} . Also, in the case of the biotin-modified dUTP derivative, the labelling efficiency estimated from the STV^{Cy3} fluorescence signals revealed that almost all phi29-DNAP variants incorporated this nucleotide into DNA hydrogels with a very similar efficiency, with the exception of phi29-ΔE, where no fluorescence signal was observed (Figure 6B). The analysis of the viscoelastic properties of the DNA hydrogels produced by phi29-DNAP with the modified dUTP analogues 2–4 showed no significant differences (Figure S12D, entries 1–4). Thus, the incorporation of small amounts of these artificial nucleotides enables the production of post-synthetically functionalizable DNA hydrogels without compromising their inherent material properties.

To investigate whether non-natural nucleotides with 2'-modifications at the ribose can also be incorporated by the phi29-DNAP variants, we performed RCA experiments by replacing 100% of the dGTP with either 2'fluoro- or 2'OMe-dGTP (5 and 6 in Figure 4, respectively). In the case of 2'OMe-dGTP analogue 6, neither the analyses by qPCR (entries 6, in Figure 5) nor by gel electrophoresis (Figure S16) showed that this nucleotide can be incorporated by any of the variants instead of the natural dGTP. Indeed, this is the case with most known polymerases, as the methoxy group impairs the proper recognition of this nucleotide as a substrate for polymerization.^[29] In contrast, all tested variants were capable of incorporating 2'fluoro-dGTP. However, the qPCR analyses showed that the RCA product concentration was about 10- to 20-fold lower than that of the natural dGTP nucleotides (see entries 1 and 5 in Figure 5). Electrophoretic analysis also confirmed that high molecular weight DNA polymer was formed, although the bands were significantly less pronounced than in the samples in which native dGTP was used (Figure S16). The apparent viscosity of the samples in which 2'fluoro-dGTP

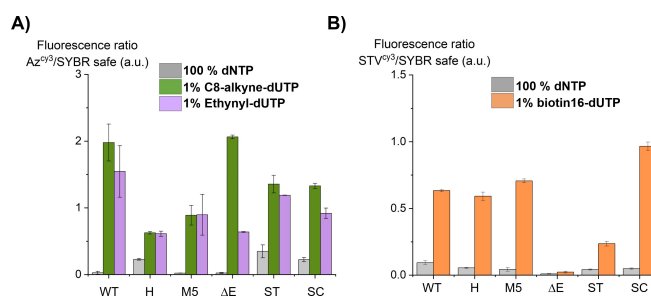


Figure 6. Estimation of the incorporation efficiency of the modified dUTP analogues by the different phi29-DNAP variants. The fluorescence intensities of the RCA product bands on an agarose gel obtained either by the DNA dye SYBR™ safe or by Az^{Cy3} or STV^{Cy3} fluorescence of the post-synthetic modification of the incorporated dUTP analogues were used to evaluate the incorporation efficiency (for schematic representation, see Figure S15). Note that the determined ratios within a gel, i.e., a particular dUTP analogue, show a high relative comparability between different phi29-DNAP variants, whereas the absolute values between different modifications (Az^{Cy3}/STV^{Cy3}) cannot be compared due to differences in coupling and fluorescence properties of the Cy3 labels. Since error bars were generated based on duplicates, no statistical significance analysis was performed.

was used instead of native dGTP was also significantly lower, suggesting that a highly cross-linked DNA hydrogel was not formed under these conditions (Figure S12D, entry 5).

Following this initial screening, we wanted to investigate the extent to which the formation of the hydrogel can be influenced by different concentrations of added 2'fluoro-dGTP. To this end, we performed RCA reactions with the phi29-WT variant using nucleotide mixtures containing different ratios of 2'fluoro-dGTP/natural dGTP (25/75, 50/50, 75/25 and 100/0%, blue bars in Figure 7A), quantified the RCA products by qPCR and compared the results with those from experiments performed in parallel in which only the corresponding amount of native dGTP was present (gray bars, in Figure 7A). The RCA products were also analyzed by agarose gel electrophoresis (Figure S17). The results showed that the additional 2'fluoro-dGTP present led to a linear increase in the additional amount of RCA products (see inset, in Figure 7A). Further investigation of the consumption of 2'fluoro-dGTP by supernatant depletion measurements using HPLC (Figures S18–S20) revealed that the absolute amount of incorporated artificial nucleotide increased linearly with higher concentrations (Figures 7B), which is consistent with the qPCR data on product formation (Figure 7A). Interestingly, considering the total amount of 2'fluoro-dGTP available for each ratio, the relative consumption showed that approximately $15 \pm 3\%$ of the artificial nucleotide was always incorporated during RCA (Figure S20C), while the native dGTP was completely consumed in all cases (Figure S20B).

Conclusions

This study compared wild-type phi29-DNAP with novel variants for RCA-based DNA hydrogel production, assessing DNA yield via qPCR and viscoelastic properties through micromechanical

indentation. Despite reports of enhanced performance, variants like phi29-H and phi29-M5 did not improve DNA amplification or yield over the wild type. The mechanical properties of the hydrogels were consistent across variants, indicating that enhanced enzyme activity in other contexts may not apply here due to the hydrogels' high DNA content and complex molecular makeup.

The new phi29-DNAP variants with protein tags (phi29-RFP, phi29-ST, phi29-SC) are particularly promising for enzyme visualization and immobilization, demonstrating strong functionality in RCA-mediated DNA hydrogel production and potential for applications like microfluidics. These variants can effectively incorporate base-modified nucleotides without significantly affecting DNA yield or hydrogel properties. However, modifications at the deoxyribose level were less successful, with 2'OMe-dGTP yielding no RCA products and 2'fluoro-dGTP showing reduced yields. Notably, this study revealed for the first time that 15% of 2'fluoro-dGTP is incorporated during RCA. Overall, from a methodological point of view, our study highlights that the combination of qPCR, electrophoresis, micromechanical indentation, and HPLC is highly effective for characterizing DNAP variants and developing new DNA-based materials for applications in materials and life sciences.

Acknowledgements

This work was financially supported through the Helmholtz Association program "Materials Systems Engineering" under the topic "Adaptive and Bioinspired Materials Systems". We thank Cornelia Ziegler for help with the purification of the enzymes, Simone Weigel with HPLC and Svenja Moench for the help with the evaluation of rheology data. Open Access funding enabled and organized by Projekt DEAL.

Conflict of Interests

The authors declare no conflict of interest.

Data Availability Statement

The data that support the findings of this study are available from the corresponding author upon reasonable request.

Keywords: Phi29 DNA polymerase · DNA hydrogel · Artificial nucleotides · Viscosity · RCA

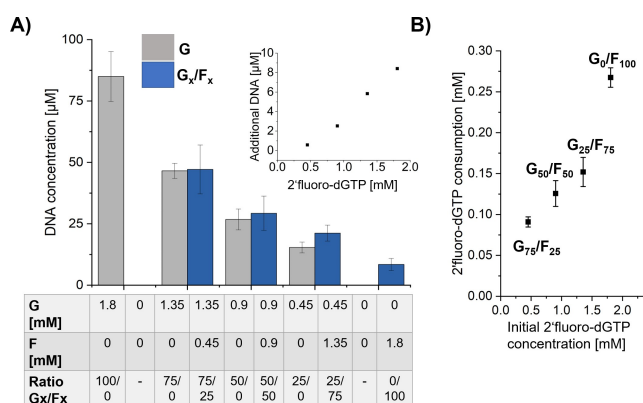


Figure 7. Influence of 2'fluoro-dGTP on the RCA process. A) qPCR quantification of RCA products generated after 72 h in reactions which contained mixtures of native dGTP (G) and 2'fluoro-dGTP (F) in varying proportions G_x/F_x (blue bars) or native dGTP only (grey bars). Error bars were determined using at least technical triplicates. The inset reflects the extra amount of RCA product that was generated due to the presence of additional 2'fluoro-dGTP. B) Amount of incorporated 2'fluoro-dGTP for the ratios tested in (A) as determined by HPLC analysis (see text for details). Since error bars were generated based on triplicates, no statistical significance analysis was performed.

- [1] N. C. Seeman, *J. Theor. Biol.* **1982**, *99*, 237–247.
- [2] a) N. C. Seeman, *Nature* **2003**, *421*, 427–431; b) M. R. Jones, N. C. Seeman, C. A. Mirkin, *Science* **2015**, *347*, 1260901; c) Y. Hu, C. M. Niemeyer, *Adv. Mater.* **2019**, *31*, e1806294.
- [3] a) D. Yang, M. R. Hartman, T. L. Derrien, S. Hamada, D. An, K. G. Yancey, R. Cheng, M. Ma, D. Luo, *Acc. Chem. Res.* **2014**, *47*, 1902–1911; b) J. Li, L. Mo, C. H. Lu, T. Fu, H. H. Yang, W. Tan, *Chem. Soc. Rev.* **2016**, *45*, 1410–1431; c) Y. Zhang, J. Tu, D. Wang, H. Zhu, S. K. Maity, X. Qu, B. Bogaert, H. Pei, H. Zhang, *Adv. Mater.* **2018**, *30*, 1703658.

- [4] S. H. Um, J. B. Lee, N. Park, S. Y. Kwon, C. C. Umbach, D. Luo, *Nat. Mater.* **2006**, *5*, 797–801.
- [5] J. B. Lee, S. Peng, D. Yang, Y. H. Roh, H. Funabashi, N. Park, E. J. Rice, L. Chen, R. Long, M. Wu, D. Luo, *Nat. Nanotechnol.* **2012**, *7*, 816.
- [6] S. A. Moench, P. Lemke, J. Weisser, I. D. Stoev, K. S. Rabe, C. M. Domínguez, C. M. Niemeyer, *Chem. Eur. J.* **2024**, *30*, e202401788.
- [7] a) Y. Hu, C. M. Domínguez, J. Bauer, S. Weigel, A. Schipperges, C. Oelschlaeger, N. Willenbacher, S. Keppler, M. Bastmeyer, S. Heißler, C. Wöll, T. Scharnweber, K. S. Rabe, C. M. Niemeyer, *Nat. Commun.* **2019**, *10*, 5522; b) Y. Hu, C. M. Domínguez, S. Christ, C. M. Niemeyer, *Angew. Chem. Int. Ed.* **2020**, *59*, 19016–19020.
- [8] a) G. Zhu, R. Hu, Z. Zhao, Z. Chen, X. Zhang, W. Tan, *J. Am. Chem. Soc.* **2013**, *135*, 16438–16445; b) R. Hu, X. Zhang, Z. Zhao, G. Zhu, T. Chen, T. Fu, W. Tan, *Angew. Chem. Int. Ed.* **2014**, *126*, 5931–5936.
- [9] a) E. Kim, L. Zwi-Dantsis, N. Reznikov, C. S. Hansel, S. Agarwal, M. M. Stevens, *Adv. Mater.* **2017**, *29*, 1701086; b) Y. Wang, E. Kim, Y. Lin, N. Kim, W. Kit-Anan, S. Gopal, S. Agarwal, P. D. Howes, M. M. Stevens, *ACS Appl. Mater. Interfaces* **2019**, *11*, 22932–22940.
- [10] a) D. Wang, Y. Hu, P. Liu, D. Luo, *Acc. Chem. Res.* **2017**, *50*, 733–739; b) M. Vázquez-González, I. Willner, *Angew. Chem. Int. Ed.* **2020**, *59*, 15342–15377; c) V. Morya, S. Walia, B. B. Mandal, C. Ghoroi, D. Bhatia, *ACS Biomater. Sci. Eng.* **2020**, *6*, 6021–6035; d) D. Wang, P. Liu, D. Luo, *Angew. Chem. Int. Ed.* **2022**, *61*, e202110666; e) R. Zhong, S. Talebian, B. B. Mendes, G. Wallace, R. Langer, J. Conde, J. Shi, *Nat. Mater.* **2023**, *22*, 818–831; lit f > R. Hama, A. Ulziibayar, J. W. Reinhardt, T. Watanabe, J. Kelly, T. Shinoka, *Biomolecules* **2023**, *13*, 280.
- [11] a) L. Blanco, A. Bernad, J. M. Lázaro, G. Martín, C. Garmendia, M. Salas, *J. Biol. Chem.* **1989**, *264*, 8935–8940; b) S. Kamtekar, A. J. Berman, J. Wang, J. M. Lázaro, M. de Vega, L. Blanco, M. Salas, T. A. Steitz, *Mol. Cell.* **2004**, *16*, 609–618.
- [12] M. Hocek, *J. Org. Chem.* **2014**, *79*, 9914–9921.
- [13] M. Hollenstein, *Org. Biomol. Chem.* **2015**, *13*, 9820–9824.
- [14] a) L. Linck, E. Reiß, F. Bier, U. Resch-Genger, *Anal. Methods* **2012**, *4*, 1215–1220; b) Ysobel R. Baker, L. Yuan, J. Chen, R. Belle, R. Carlisle, Afaf H. El-Sagheer, T. Brown, *Nucleic Acids Res.* **2021**, *49*, 9042–9052.
- [15] J. A. Esteban, M. Salas, L. Blanco, *J. Biol. Chem.* **1993**, *268*, 2719–2726.
- [16] a) S. Tang, H. Wei, T. Hu, J. Jiang, J. Chang, Y. Guan, G. Zhao, *Biosci. Biotechnol. Biochem.* **2016**, *80*, 1555–1561; b) J. Jakubovska, D. Tauraitė, L. Birštonas, R. Meškys, *Nucleic Acids Res.* **2018**, *46*, 5911–5923.
- [17] M. de Vega, J. M. Lázaro, M. Mencía, L. Blanco, M. Salas, *Proc. Nat. Acad. Sci.* **2010**, *107*, 16506–16511.
- [18] T. Povilaitis, G. Alzbutas, R. Sukackaite, J. Siurkus, R. Skirgaila, *Protein Eng. Des. Sel.* **2016**, *29*, 617–628.
- [19] L. L. Torres, V. B. Pinheiro, *Curr. Protoc. Chem. Biol.* **2018**, *10*, e41.
- [20] A. Khvorova, J. K. Watts, *Nat. Biotechnol.* **2017**, *35*, 238–248.
- [21] M. de Vega, J. M. Lázaro, M. Salas, L. Blanco, *EMBO J.* **1996**, *15*, 1182–1192.
- [22] a) H. Cao, X. Zhou, Y. Zeng, *Sens. Actuators B: Chem.* **2019**, *279*, 447–457; b) Y. Guo, W. Li, R. Zhang, S. Cao, X. Zhu, G. Chen, C. Feng, *Lab. Chip.* **2023**, *23*, 2601–2610; c) P. Lemke, L. Schneider, W. Kunz, A. L. Rieck, P. S. Jäger, A. Bruckmann, B. Nestler, K. S. Rabe, C. M. Niemeyer, *Adv. Funct. Mater.* **2024**, *34*, 2313944.
- [23] A. H. Keeble, M. Howarth, *Chem. Sci.* **2020**, *11*, 7281–7291.
- [24] L. Schneider, M. Richter, C. Oelschlaeger, K. S. Rabe, C. M. Domínguez, C. M. Niemeyer, *Chem. Commun.* **2023**, *59*, 12184–12187.
- [25] P. Lemke, S. Moench, P. S. Jäger, C. Oelschlaeger, K. S. Rabe, C. M. Domínguez, C. M. Niemeyer, *Small Methods* **2024**, 2400251.
- [26] P. Pérez-Arnaiz, J. M. Lázaro, M. Salas, M. de Vega, *Nucleic Acids Res.* **2006**, *34*, 3107–3115.
- [27] T. Peschke, M. Skoupi, T. Burgahn, S. Gallus, I. Ahmed, K. S. Rabe, C. M. Niemeyer, *ACS Catal.* **2017**, *7*, 7866–7872.
- [28] a) T. Ono, M. Scaff, L. M. Smith, *Nucleic Acids Res.* **1997**, *25*, 4581–4588; b) Z. Liu, T. Chen, F. E. Romesberg, *Chem. Sci.* **2017**, *8*, 8179–8182.
- [29] F. Wang, P. Li, H. C. Chu, P. K. Lo, *Biosensors* **2022**, *12*, 93.
- [30] D. G. Gibson, L. Young, R. Y. Chuang, J. C. Venter, C. A. Hutchison, H. O. Smith, *Nat. Methods* **2009**, *6*, 343–345.
- [31] R. Merindol, G. Delechiave, L. Heinen, L. H. Catalani, A. Walther, *Nat. Commun.* **2019**, *10*, 528.
- [32] J. P. Hannan, G. H. Swisher, J. G. Martyr, N. J. Cordaro, A. H. Erbse, J. J. Falke, *Anal. Biochem.* **2021**, *631*, 114338.
- [33] M. Zuker, *Nucleic Acids Res.* **2003**, *31*, 3406–3415.

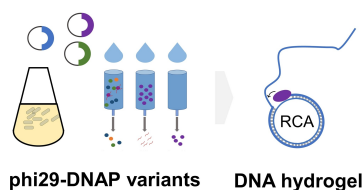
Manuscript received: August 13, 2024

Accepted manuscript online: October 8, 2024

Version of record online: ■■, ■■

RESEARCH ARTICLE

New phi29 DNA polymerase variants for RCA-based DNA hydrogel production are developed, featuring modified binding properties and the ability to incorporate non-natural nucleotides with potential for generating advanced materials. Their synthesis performance and the ability to incorporate various non-natural nucleotides modified at the nucleobase or sugar moiety for the production of DNA hydrogels are evaluated and comprehensively characterized by qPCR, micromechanical indentation, and HPLC



*P. Gaspers, P. Lemke, A. Delavault, C. M. Domínguez, K. S. Rabe, C. M. Niemeyer**

1 – 10

Engineering Phi29-DNAP Variants for Customized DNA Hydrogel Materials

